Nanoporous Materials

A Self-Ordered, Crystalline–Glass, Mesoporous Nanocomposite for Use as a Lithium-Based Storage Device with Both High Power and High Energy Densities**

Haoshen Zhou, Donglin Li, Mitsuhiro Hibino, and Itaru Honma*

Lithium-based storage devices with both high power and high energy densities are necessary for electric devices, especially for electric vehicles (EV) and other mobile or portable electric devices.[1] Herein we introduce a new concept to design a novel electrode material having a self-ordered, crystalline-glass, mesoporous nanocomposite (CGMN) structure for such industrial needs. The 5-nm frameworks of the CGMN are assembled in a compact arrangement from electrode-active nanocrystals with a small quantity of glass phase. The 4-nm uniform mesochannels of the CGMN can be filled with electrolyte solution during use to provide electrolyte and lithium-ion pathways throughout the material. In addition, the high surface area of the CGMN reduces the effective specific current density, and the three-dimensional glass network in the framework of the CGMN is able to incorporate a high content of electronic conductive oxides above the percolation-threshold value to form an electronic path, and to add lithium ions as a network modifier during the first insertion process to form an ionic path. The experimental results show that the specific capacities (energy density) at high current densities (power density) can be improved several hundred fold when the CGMN replaces TiO_2 powder as the electrode of a lithium-based storage device.

An electric vehicle (EV) powered by a rechargeable battery is an ideal solution to reduce environmental pollution as it is a clean energy source. However, the power densities of rechargeable batteries are still too low to support such industrial needs, even though their energy densities are high. The development of such an energy-storage device with both high power and high energy densities has been widely studied.[1] There are two typical approaches in this field: one is to increase the energy density of the capacitor, which is often studied by measurement of the electrical double-layer capacity (EDLC), and the other is to improve the specific capacity of the rechargeable battery by a rapid charge–discharge process, especially for lithium-based rechargeable batteries. Recently, a great deal of effort has been spent on improving the energy density of the EDLC by increasing the effective surface area of carbon-based materials,[2] although the resulting densities are still too low. In the second approach there are four main problems that have to be solved:[3,4] a) the particle size needs to be decreased to reduce the required diffusion length in the active materials; b) the effective specific current density needs to be reduced in the rapid charge–discharge process; c) a high cycle performance needs to be achieved even during the rapid charge–discharge process; and d) the electronic conductivity of the electrode materials needs to be increased.

The diffusion of lithium ions is very complex because the nature of the electrolyte phase, the solid–liquid interface, the tortuosity, and the size of the nanoparticles have to be considered.[5] Herein we only consider the the overall process by assuming that the diffusion coefficient is independent of these factors, which means that the diffusion length, L, can be estimated as $\sqrt{D\tau}$,[6] where D and τ are the diffusion coefficient and time, respectively. The value of τ decreases rapidly at high charge–discharge current, so the effective specific capacity rate will depend on the volume ratio $[r^3-(r-L)^3]/r^3$, where r is the radius of the active particle (Figure 1a). The required diffusion length L should be larger than r (namely, $L(=\sqrt{D\tau}) \geq r$) to obtain the maximum specific capacity. If we assume that the rapid charge–discharge process is complete within one minute and that D is of the order of $10^{-16}\,cm^2\,s^{-1}$ [5] in the solid state, particles with a size of $2r$ should be about 2 nm. If it is assumed that a particular material is constructed in a compact manner from nanoparticles with a size of 2 nm, most of the pores in the material should be micropores with a pore size in the range of 0.5 to 1.0 nm, and therefore much of the internal surface area of the solid will not be accessible to electrolyte solutions containing the large organic solvent molecules usually used to dissolve the lithium ions. Herein, we report the synthesis of a novel, self-ordered, mesoporous nanocomposite (CGMN) to satisfy such needs.

[*] Dr. H. Zhou, Dr. D. Li, Dr. M. Hibino, Dr. I. Honma
Institute of Energy Technology
National Institute of Advanced Industrial Science and Technology (AIST)
Umezono 1-1-1, Tsukuba, 305-8568 (Japan)
Fax: (+81) 298-615-829
E-mail: hs.zhou@aist.go.jp

[**] H.Z. thanks Mr. Mitsuhiro Ichihara for his help with the TEM observations, as well as the Japanese Society for the Promotion of Science (JSPS) and the National Institute of Advanced Industrial Science and Technology (AIST) for partially funding this research. D.L. acknowledges the financial support of a JSPS Fellowship for work carried out at the Institute of Energy Technology.

Supporting information for this article is available on the WWW under http://www.angewandte.org or from the author.

 DOI: 10.1002/ange.200460937

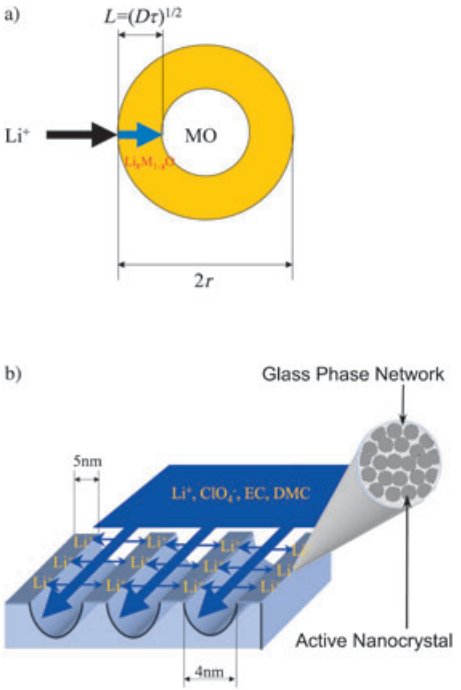

Figure 1. a) A schematic representation of the effective diffusion length in electrode-active materials. The area marked in yellow shows the volume reacting with Li^+ ions in the charge/discharge period τ in a diffusion-controlled process. b) A schematic representation of the reduced diffusion length in a rechargeable battery containing a self-ordered CGMN.

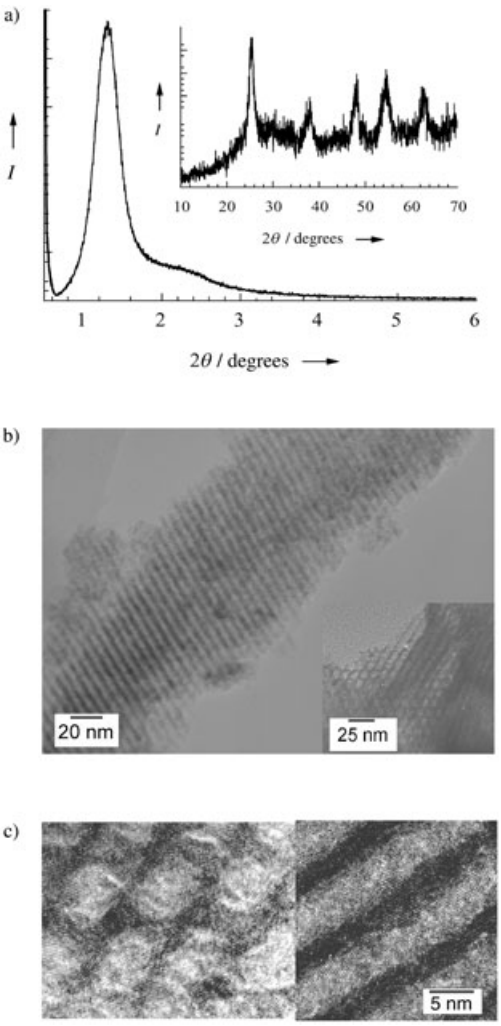

Figure 2. a) The small-angle X-ray diffraction (SAXRD) patterns and wide-angle X-ray diffraction (WAXRD) patterns of TiO_2–P_2O_5 CGMN (inset). b) TEM images of the self-ordered mesoporous structure. c) High-resolution TEM images of the TiO_2–P_2O_5 CGMN perpendicular to (left), and along the direction of (right), the nanochannels.

Self-ordered mesoporous materials were first reported in 1992,[7] and have since found applications in catalysis, absorbents, separation technology, gas sensors, solar cells, and electronics.[8–10] The framework of the self-ordered, mesoporous metal oxide is generally in an amorphous state because the crystallization of the metal oxide at high temperatures causes the collapse of the self-ordered, mesoporous structure. However, most cathode- and anode-active oxides with stable charge–discharge performance are active in the crystalline phase, such as $LiMn_{2-x}M_xO_4$ (M = transition metal)[11] in the spinel phase, $LiMPO_4$ (M = Mn, Fe, Co, Ni)[11] with an olivine structure, TiO_2 with an anatase structure, and TiS_2, $LiCoO_2$, and $LiMnO_2$ with a layer structure.[11] Recently, we designed and synthesized a CGMN with a high thermal stability that contains a homogeneous, nanocrystalline metal oxide assembled in the framework.[12] Herein, we have chosen TiO_2 as the nanocrystalline transition-metal oxide for potential application as the anode of a lithium-based rechargeable battery.[13–15] In addition, a phosphate-based glass was selected as the glass phase to construct TiO_2–P_2O_5 (CGMN).[12]

The TiO_2–P_2O_5 CGMN is a two-dimensional, hexagonal mesostructure with a unit cell length of 11 nm (Figure 2a). It contains uniform pores with a diameter of 4 nm (see TEM image in Figure 2b) and a framework of 5-nm width that are co-assembled with 3–5-nm nanocrystalline anatase TiO_2 particles (see WAXRD image in the inset of Figure 2a and the high-resolution TEM image in Figure 2c). Such a CGMN has five novel characteristics—uniform nanochannels, a uniform nanoframework, a high surface area, a glass-phase buffer layer, and an electronic network path—that suggest its possible use as an electrode to overcome the main problems for a lithium-based storage device with both high power and high energy densities.

The first two novel characteristics of the CGMN are the uniform nanochannel and the framework with an electrode-active nanocrystal. A uniform channel 4 nm wide is large enough to be easily accessed by an electrolyte solution that includes large organic molecules such as ethylene carbonate (EC) or dimethoxyl carbonate. Li^+ ions and counteranions such as ClO_4^- can be transported inside the CGMN and react with the nanocrystalline metal-oxide framework, which is assembled from 3–5 nm TiO_2 anatase nanocrystals. In this case, the required diffusion length for the lithium ions could be reduced to half of the frame-wall thickness, about 2 nm (Figure 1b). This arrangement guarantees that a rapid charge–discharge process will be complete in a very short period of time, which results in a high specific capacity even at

a high charge–discharge current. The charge–discharge profiles of the TiO_2–P_2O_5 CGMN at different current densities are shown in Figure 3a. Both the discharge and charge processes show similar specific capacities of about 260 mA h g^{-1} at a current density of 10 A g^{-1}. We assume that TiO_2 is the only active material, even though acetylene/black carbon (AB) and P_2O_5 are present in the electrode materials, since the specific capacities of pure AB and pure P_2O_5 are too small to be measured at a current density of 10 A g^{-1}.[16] The insertion and extraction process can be described by $TiO_2 + x(Li^+ + e^-) \rightleftharpoons Li_xTiO_2$.[13,15] The specific capacity of traditional anatase (TiO_2) dramatically decreases at a high current density because the over-potential from the various polarizations is very large at high current density.

We also investigated traditional anatase (TiO_2) which was purchased in powder (PP) form with a particle size of several hundred nanometers. The specific capacity of this powder was less than 1 mA h g^{-1} at 10 A g^{-1}. A mesoporous TiO_2 powder (MP), which was synthesized by the method of Stucky and coworkers,[17] had an activity of about 18 mA h g^{-1} at 10 A g^{-1} (Figure 3c). In our CGMN system we find a specific capacity of 260 mA h g^{-1} for anatase TiO_2 at a current density of 10 A g^{-1}. This extremely large value corresponds to $x = 0.76$ for Li_xTiO_2, which is much larger than the highest value ($x = 0.5$; 167.5 mA h g^{-1}) previously reported for anatase Li_xTiO_2.[15] It has been reported recently that there are two reduction/oxidation models for self-ordered, mesoporous TiO_2:[18] one is the traditional insertion/extraction of Li^+ ions into Li_xTiO_2, and the other is surface storage of Li, which has been observed in mesoporous, nanosheet, and nanorod TiO_2,[18] although the exact mechanism is still unknown. In the cyclic voltammogram (CV) of the TiO_2–P_2O_5 CGMN, the peaks of both Li^+ ion insertion/extraction and surface storage of Li are observed at 1.7/1.9 eV and 1.5/1.6 eV (Li^+/Li), respectively (Figure 3b). It is therefore reasonable for the total specific energy capacity of the TiO_2–P_2O_5 CGMN to be much larger than the maximum value of $x = 0.5$ for insertion of Li^+ ions into anatase TiO_2.

The third novel characteristic of the CGMN is its high surface area (about 280 m^2 g^{-1}),[12] which reduces the specific current density from I/A_{area} to I/S_{area}, where A_{area} and S_{area} are the areas of the nickel-mesh electrode and the surface area of the TiO_2–P_2O_5 CGMN, respectively. If it is considered that A_{area} (0.25 cm^2) and S_{area} (2.8×10^3 cm^2 for 1 mg of the TiO_2–P_2O_5 CGMN) differ by a factor of 10^4, the effective current density (I/S_{area}) is about 10^{-4} of the practical applied current density of an electrode (I/A_{area}); this is why the specific capacity remains very high even at the high charge–discharge

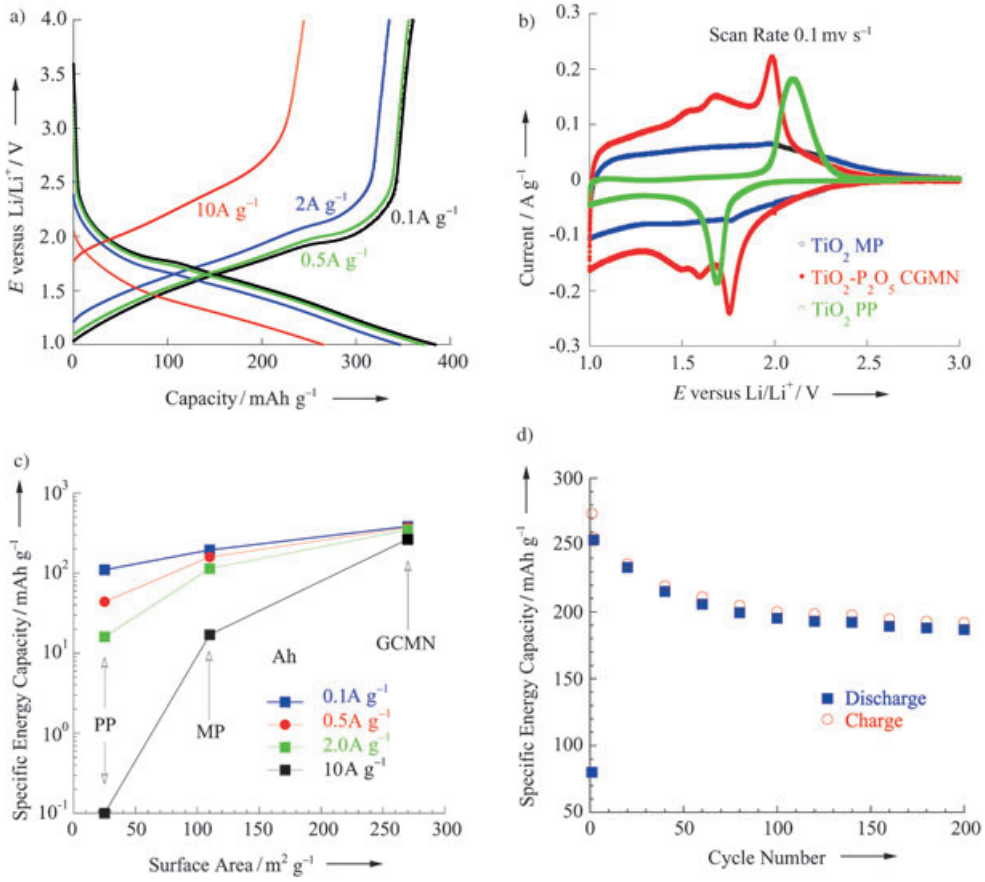

Figure 3. a) The second cycle charge–discharge profiles of the TiO_2–P_2O_5 CGMN in the potential range from 1.0 to 4.0 V (versus Li^+/Li) with current densities of 0.1, 0.5, 2, and 10 A g^{-1} based on active TiO_2. b) The cyclic voltammetry (CV) curves of the TiO_2–P_2O_5 CGMN, TiO_2 MP, and TiO_2 PP at a scan speed of 0.1 mv s^{-1} in a potential window from 1.0 to 3.5 eV (versus Li^+/Li). c) The relationship between specific energy capacity and the surface area at current densities of 10, 2, 0.5, and 0.1 A g^{-1}. d) The performance cycle of discharge and charge capacities of TiO_2–P_2O_5 CGMN at a current density of 10 A g^{-1}.

current density for the TiO_2-P_2O_5 CGMN with a high surface area (Figure 3c). It is also the reason why the specific capacity dramatically decreases at high charge–discharge current density for TiO_2 PP with a low surface area of about 25 $m^2 g^{-1}$ (Figure 3c). The high specific capacity at a high charge–discharge current density is therefore a result of the decrease in the required diffusion length (about 2 nm) and of the decrease in the effective current density (I/S_{area}).

The fourth novel characteristic is that the P_2O_5-glass phase forms a buffer layer between active nanocrystalline TiO_2 blocks that helps to relax the stress because of the insertion and extraction of lithium ions and thereby improves the performance cycle under rapid charge–discharge conditions. Lithium insertion and extraction generally results in a small change in the crystalline lattice length. This small change destroys both the nanoarchitecture and the crystalline structure, and results in poor performance after a number of charge–discharge cycles.[4] Our TiO_2–P_2O_5 CGMN gives good performance up to 200 cycles, with a specific capacity of about 195 mA h g^{-1} (see Figure 3d), and has a high coulomb efficiency of 96%. The specific capacity remains at about 150 mA h g^{-1}, with a high coulomb efficiency of 93%, up to the 800th cycle.

The final and very important characteristic of the CGMN is that the P_2O_5-glass phase can also act as a host for electronic conductive oxide dopants to build up an ideal electronic path throughout the material. Recently, a large number of binary and ternary glasses with electronic and ionic conductivities (containing transition-metal oxides) have been investigated for possible practical applications as solid-state lithium-ion batteries and integrated microbatteries,[19,20] We have doped metal oxides (M_xO_y; Li_2O, NiO, CuO, Fe_2O_3, MnO_2, SnO_2, WO_3) into P_2O_5 to form ternary M_xO_y–P_2O_5 composites containing some residual TiO_2-glass network.[12] The incorporation of an electronically conductive oxide, such as CuO or SnO_2, into the three-dimensional network of the P_2O_5-glass phase, to form a multicomponent P_2O_5–CuO–TiO_2 or P_2O_5–SnO_2–TiO_2 glass path inside the TiO_2–P_2O_5–CuO or TiO_2–P_2O_5–SnO_2 CGMN respectively, improved the electronic conductivity of TiO_2–P_2O_5 CGMN. According to inductively coupled plasma (ICP) analysis, the incorporation ratio of CuO or SnO_2 into P_2O_5 was about 0.20 and 0.44, respectively. These values are high enough to form an electronically conductive CuO or SnO_2 path in the P_2O_5-glass network with a percolation-threshold value in the range 0.13–0.18.[21] We also synthesized a TiO_2–SiO_2 CGMN system.[12] The experimental results show this system has a worse performance than TiO_2–P_2O_5 CGMN,[16] which indicates that SiO_2-glass networks are poorer electronic conductors than a P_2O_5-glass network. CuO or SnO_2 is incorporated into the P_2O_5-glass phase as a result of the interaction of the P=O bond, in the form of PO_4 anions, with metal ions.[12,22] Moreover, during the discharge process, when lithium ions insert into the active materials, some lithium ions also diffuse into the glass networks to form multicomponent Li_2O–CuO–P_2O_5–TiO_2 and Li_2O–SnO_2–P_2O_5–TiO_2 glassy network systems. In fact, according to recent results,[20] ternary and multicomponent glasses show both an electronic conductive path, because of the presence of transition-metal oxides, and an ionic path, arising from the alkali-metal oxides. Both these factors improve the lithium storage performance. For example, the specific capacity of a TiO_2–P_2O_5 CGMN (65 mA h g^{-1}) at a current density of 20 A g^{-1} is improved significantly to 195 mA h g^{-1} for TiO_2–P_2O_5–SnO_2 CGMN and 270 mA h g^{-1} for TiO_2–P_2O_5–CuO (Figure 4a). The charge–discharge profiles of the TiO_2–P_2O_5–SnO_2 CGMN at current densities of 10 A g^{-1}, 20 A g^{-1}, and 50 A g^{-1} are 230 mA h g^{-1}, 195 mA h g^{-1}, and 178 mA h g^{-1}, respectively (Figure 4a).

The relationship between the specific capacities of discharge and the current densities of the TiO_2 PP, TiO_2 MP, TiO_2–P_2O_5 CGMN, TiO_2–P_2O_5–CuO CGMN, and TiO_2–P_2O_5–SnO_2 CGMN are shown in Figure 4b. The specific capacity of traditional TiO_2 anatase particles at 10 A g^{-1} is increased several hundred times upon incorporation into a TiO_2–P_2O_5 CGMN. Furthermore, the specific capacity of the TiO_2–P_2O_5 CGMN at 20 A g^{-1} is further improved by a factor of about four or five upon formation of a TiO_2-P_2O_5-CuO CGMN or TiO_2-P_2O_5-SnO_2 CGMN.

The energy density E and power density P in a constant-current charge–discharge can be written as: $E = \int_0^{\tau_d} \frac{IV}{m} dt = \frac{I}{m} V_{av} \tau_d$ and $P = \frac{1}{\tau_d} \int_0^{\tau_d} \frac{IV}{m} dt = \frac{I}{m} V_{av}$, where, I, V, and m are the current, cell voltage, and mass of active material, respectively. τ_d and V_{av} are the average discharge (or charge) time and average potential, respectively. For the power-density and energy-density calculations, we assume that the TiO_2–P_2O_5 CGMN will be used as the anode with V_2O_5[3] as the cathode (ca. 3.5 V versus Li/Li^+, 250 mA h g^{-1} at 10 A g^{-1}). These equations give a value of V_{av} of 1.65 V. The weight, including all other parts of the battery such as the current collector, electrolytes, and chassis, is assumed to be five times that of the active materials. The calculated[23] energy densities and power densities of these CGMN lithium-based storage devices are higher than the targets of PNGV (the Partnership for a New Generation of Vehicle)[1] (Figure 4c).

The experimental results described here show that the five novel characteristics—uniform nanochannels, uniform nanoframework, high surface area, glass-phase buffer layer, and electronic network path—of this GCMN suggest its suitability for the development of high power and high energy density lithium-based storage devices. These results are interesting with respect to both fundamental research and potential applications. We first introduced a lithium-ion pathway through the nanochannels and an electronic pathway through the three-dimensional, glass-phase network by assembling nanocrystals into the electrode materials to give a GCMN structure that is able to undergo a rapid charge–discharge process, which differs from the traditional concept of lithium-ion insertion/extraction into bulk crystalline materials. We hope this concept can be extended to electrode-active materials such as Si and Sn, for the anode, and LiM_2O_4 (M = transition metal) and $LiMPO_4$ (M = Mn, Fe, Co, Ni, etc) for the cathode, by functionalization with Si, Sn, LiM_2O_4, and $LiMPO_4$ CGMNs. This will be of benefit not only to the EV industry, but also to any other mobile or portable electronic device, for saving charging time.

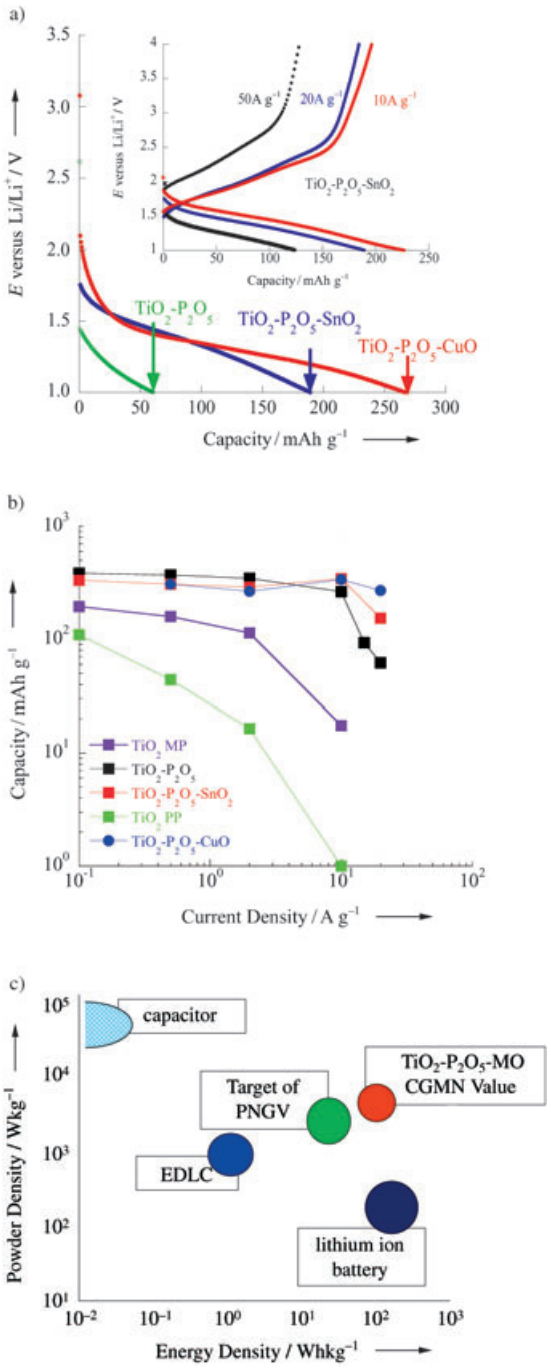

Figure 4. a) The charge–discharge profiles of the TiO_2–P_2O_5 CGMN, TiO_2–P_2O_5–SnO_2 CGMN and TiO_2–P_2O_5–CuO CGMN at 20 $A\,g^{-1}$. The inset shows that the specific capacity of the TiO_2–P_2O_5–SnO_2 CGMN at current densities of 10 $A\,g^{-1}$, 20 $A\,g^{-1}$, and 50 $A\,g^{-1}$ is 230, 195, and 178 $mA\,h\,g^{-1}$, respectively. b) The relationship between the specific discharge capacities and the current densities of TiO_2–P_2O_5 CGMN, TiO_2–P_2O_5–SnO_2 CGMN, and TiO_2–P_2O_5–CuO CGMN. c) A Regone plot showing the position of the power and energy densities of CGMN, including all components, as an energy-storage device, relative to EDLC, a capacitor, a traditional rechargeable lithium battery, and the PNGV target.

Experimental Section

Titanium tetraisopropoxide (TTIP, 2.5 g) was added to a solution of triblock copolymer $HO(CH_2CH_2O)_{20}(CH_2CH(CH_3)O)_{70}(CH_2CH_2O)_{20}H$ (P123; 0.8–1.2 g) in ethanol (8–10 g). The mixture was stirred for 10 mins and 0.5 N HCl (1 g) added to form a transparent solution. $PO(C_2H_5)_3$ (1 g) was then added to this solution. In the case of doped materials, 10 mol % $CuCl_2$ or $SnCl_4$ was added with stirring. The multicomponent mixtures were stirred in a sealed bottle for 20 h. The transparent sols were then gelled in an open petri dish at room temperature in air for 5 days to give a transparent gel that was then dried at 80 °C for 7 days. The as-synthesized samples were calcined at 400 °C for 6 h to remove any organic species and afforded inorganic amorphous solids. These products were subsequently annealed at 500 °C for 1–2 h under air to form the desired nanocomposites.

Powder X-ray diffraction (XRD) patterns were recorded on a MacScience-M03XHF22 diffractometer using $Cu_{K\alpha}$ irradiation. The nitrogen adsorption/desorption isotherm curve was recorded at 77 K on a Belsorpt-23SA volumetric adsorption analyzer. The BET surface area was calculated from the adsorption/desorption isotherm curve. TEM studies were carried out at 200 Kev on a Hitachi-800 instrument. Inductively coupled plasma analyses were performed on a Therm Jarrell Ash IRIS/AP instrument.

For electrochemical measurement, the samples were heated at 120 °C in a vacuum for 5 h to remove adsorbed water on the surface of the mesopore. They were then mixed and ground with 5 wt % teflon (poly(tetrafluoroethylene)) powder as a binder and 45 wt % acetylene back carbon (AB) powder as the conductive assistant materials. The mixture was spread and pressed on a 0.25 cm^2 nickel mesh (100 mesh) as the working electrode (WE). The reference (RE) and counter electrode (CE) were prepared by spreading and pressing lithium metals on such a nickel mesh. The electrolyte was 1 M $LiClO_4$ in EC + DMC (EC/DMC = 1/1 v/v). Cell assembly was carried out in a glove box under an argon atmosphere. The charge-discharge performance of the material was investigated in such a three-electrode cell using lithium metal as the counter and reference electrodes.

Cyclic voltametry studies were performed over a potential range of 1.0 to 3.5 V (Li^+/Li) at scan rates of 0.1, 0.5, 2, 10, and 50 $mv\,s^{-1}$. Galvanostatic discharge-charge was performed in a potential range of 1.0 to 4.0 V (Li^+/Li) under constant currents of 0.1, 0.5, 2, 10, 20, and 50 $A\,g^{-1}$. The circuit was kept open for 10 min after each discharge and charge. The weight was based on the active materials (TiO_2, excluding P_2O_5 and AB), unless otherwise noted. The TiO_2 content is about 85 wt % in TiO_2–P_2O_5 CGMN.

Received: June 11, 2004
Revised: August 26, 2004
Published online: December 21, 2004

Keywords: conducting materials · lithium storage · materials science · mesoporous materials · nanostructures

[1] B. Scrosati, *Nature* **1995**, *373*, 557; R. F. Nelson, *J. Power Sources* **2000**, *91*, 2.
[2] K. Sawai, T. Ohzuku, *J. Electrochem. Soc.* **1997**, *144*, 988.
[3] T. Kudo, Y. Ikeda, T. Watanabe, M. Hibino, M. Miyayama, H. Abe, K. Kajita, *Solid State Ionics* **2002**, *152–153*, 833.
[4] M. Hibino, H. Kawaoka, H. S. Zhou, I. Honma, *J. Power Sources* **2003**, *124*, 143; H. Kawaoka, M. Hibino, H. S. Zhou, I. Honma, *J. Power Sources* **2004**, *125*, 85.
[5] L. Kavan, J. Prochazka, T. M. Spitler, M. Kalbac, M. Zukalova, T. Drezen, M. Gratzel, *J. Electrochem. Soc.* **2003**, *150*, A1000.
[6] J. Bard, L. R. Faulkner, *Electrochemical Methods*, Wiley, New York, **1980**.
[7] C. T. Kresge, M. E. Leonowicz, W. J. Roth, J. C. Vartuli, J. S. Beck, *Nature* **1992**, *359*, 710.
[8] M. E. Davis, *Nature* **2002**, *417*, 813; A. Stein, *Adv. Mater.* **2003**, *15*, 763; R. D. Miller, *Science* **1999**, *286*, 421; U. Bach, D. Lupo, P.

Comte, J. E. Moster, F. Weissortel, J. Salbeck, H. Spreitzer, M. Gratzel, *Nature* **1998**, *395*, 583.
[9] T. Yamada, H. S. Zhou, H. Uchida, M. Tomida, Y. Ueno, T. Ichino, I. Honma, K. Asai, T. Katsube, *Adv. Mater.* **2002**, *14*, 812; Y. Ueno, T. Horiuchi, M. Tomita, O. Niwa, H. S. Zhou, T. Yamada, I. Honma, *Anal. Chem.* **2002**, *74*, 5257.
[10] H. S. Zhou, S. Zhu, M. Hibino, I. Honma, M. Ichihara, *Adv. Mater.* **2003**, *15*, 2107.
[11] M. Winter, J. O. Besenhard, M. E. Spahr, P. Novak, *Adv. Mater.* **1998**, *10*, 725; M. Wakihara, O. Yamamoto, *Lithium Ion Batteries*, Wiley-VCH, Weinheim, **1988**.
[12] D. Li, H. S. Zhou, I. Honma, *Nature Mater.* **2004**, *3*, 65.
[13] L. Kavan, M. Gratzel, S. E. Gilbert, C. Klemenz, H. J. Scheel, *J. Am. Chem. Soc.* **1996**, *118*, 6716.
[14] J. M. Tarascon, M. Armand, *Nature*, **2001**, *414*, 359; S. Y. Huang, L. Kavan, I. Exnar, M. J. Gratzel, *J. Electrochem. Soc.* **1995**, *142*, L142.
[15] M. Wagemaker, A. P. M. Kentgens, F. M. Mulder, *Nature* **2002**, *418*, 397.
[16] H. S. Zhou, D. Li, M. Hibino, I. Honma, unpublished results.
[17] P. Yang, D. Zhao, D. I. Margolese, B. F. Chmelka, G. D. Stucky, *Nature* **1998**, *396*, 152; P. Yang, D. Zhao, D. I. Margolese, B. F. Chmelka, G. D. Stucky, *Chem. Mater.* **1999**, *11*, 2813.
[18] L. Kavan, J. Rathousky, M. Gratzel, V. Shklover, A. Zukal, *J. Phys. Chem. B* **2000**, *104*, 12012; L. Kavan, J. Rathousky, M. Gratzel, V. Shklover, A. Zukal, *Microporous Mesoporous Mater.* **2001**, *44–45*, 653; L. Kavan, M. Kalbac, M. Zukalova, I. Exnar, V. Lorenzen, R. Nesper, M. Gratzel, *Chem. Mater.* **2004**, *16*, 477; X. Gao, H. Zhu, G. Pan, S. Ye, Y. Lan, F. Wu, D. Song, *J. Phys. Chem. B* **2004**, *108*, 2868; M. Wagemaker, G. J. Kearley, A. A. VanWell, H. Mutka, F. M. Mulder, *J. Am. Chem. Soc.* **2003**, *125*, 840.
[19] M. M. El-Desoky, *Mater. Chem. Phys.* **2002**, *73*, 259; L. Bih, M. El Omari, J. M. Reau, A. Nadiri, A. Yacoubi, M. Haddad, *Mater. Lett.* **2001**, *50*, 308.
[20] J. E. Garbarczyk, M. Wasiucionek, P. Machowski, W. Jakubowski, *Solid State Ionics* **1999**, *119*, 9; L. Bih, M. El Omari, J. M. Reau, M. Haddad, D. Boudlich, A. Yacoubi, A. Nadiri, *Solid State Ionics* **2000**, *132*, 71.
[21] D. S. McLachlan, M. Blaszkiewicz, R. E. Newnham, *J. Am. Ceram. Soc.* **1990**, *73*, 2187.
[22] The typical small-angle X-ray diffraction (SAXRD) peaks from the hexagonal mesoporous structure and the broad wide-angle X-ray diffraction (WAXRD) peaks of TiO_2 anatase nanocrystals are still clearly present after incorporation of CuO or SnO_2 into the P_2O_5-glass phase. We did not observe any compounds with the structure $Ti_{1-x}Cu_{2x}O_2$ or $Ti_{1-x}Sn_xO_2$ in the TiO_2–P_2O_5–CuO or TiO_2–P_2O_5–SnO_2 CGMNs, respectively.
[23] B. E. Conway, *Electrochemical Supercapacitors*, Kluwer Academic Publishers, Plenum, New York, **1999**.

